Comparison of the Single-Wavelength and Spectral-Reconstruction Methods for Determining the Solvation-Response Function

ARTICLE *in* THE JOURNAL OF PHYSICAL CHEMISTRY A · FEBRUARY 1999

Impact Factor: 2.69 · DOI: 10.1021/jp984004q

2 AUTHORS:

Joseph Gardecki
Massachusetts General Hospital
36 PUBLICATIONS **2,882** CITATIONS
SEE PROFILE

Mark Maroncelli
Pennsylvania State University
126 PUBLICATIONS **11,750** CITATIONS
SEE PROFILE

Comparison of the Single-Wavelength and Spectral-Reconstruction Methods for Determining the Solvation-Response Function

J. A. Gardecki and M. Maroncelli*

Department of Chemistry, The Pennsylvania State University, University Park, Pennsylvania 16802

Received: October 8, 1998; In Final Form: December 14, 1998

A comparison of the solvation/spectral-response functions obtained by two independent techniques, the single-wavelength and spectral-reconstruction methods, is reported. Determination of the best wavelengths for application of the linear-single-wavelength approximation for the solute coumarin 153 (C153) is achieved using radiative rate data and steady-state emission spectra in a series of 36 different solvents at room temperature. The optimal linear wavelength is found to be 555 nm. (This wavelength, which is on the red side of the spectrum, yields superior results when compared to the more traditional choice of 470−480 nm, on the blue side.) Response functions determined using both 560- and 470-nm observation wavelengths are compared to previously reported spectral-reconstruction results in 24 solvents. A comparison of the characteristic times indicates that the linear-single-wavelength method can be used to predict solvation times with an accuracy of roughly ±30−40% (1 standard deviation) using suitably scaled data collected at ∼560 nm. Application of a nonlinear version of the single-wavelength method does not provide increased accuracy.

I. Introduction

Continuing interest in polar solvation dynamics[1,2] is driven by the recognition that these dynamics are important for understanding a range of condensed-phase processes. Examples are ion mobility,[3] rotational[4,5] and vibrational relaxation,[6,7] and solution-phase chemical reaction.[8,9] For this reason, different workers have employed a variety of techniques such as transient hole burning,[10,11] absorption,[12] photon echo,[13−16] transient grating,[16,17] and optical Kerr[15,18] spectroscopies to characterize time-dependent solvation processes. The most direct method, and the one examined here, is based on monitoring the time-dependent fluorescence Stokes shift of a probe solute.[1,2,19−23]

Prior to excitation by an ultrafast laser pulse, the ground electronic state of the solute is in dynamic equilibrium with a distribution of solvent states (configurations). Upon excitation, the charge density of the solute is instantaneously switched to that of the excited state, resulting in a change of the magnitude and direction of the solute's dipole moment. Solvent molecules near the probe, which are frozen on the time scale of the excitation, respond via rotational, vibrational, and translational motions in order to optimize their interactions with the new solute charge distribution. The solute monitors this dynamical response via a shift of its emission frequency to lower energy. This "dynamic Stokes shift" is typically represented by the normalized spectral response function, $S_\nu(t)$

$$S_\nu(t) \equiv \frac{\nu(t) - \nu(\infty)}{\nu(0) - \nu(\infty)} \tag{1}$$

where $\nu(0)$ and $\nu(\infty)$ are the frequency of the emission spectrum immediately after excitation by a laser pulse and when equilibrium has been reestablished, respectively.

The above description of the time-dependent Stokes shift experiment implies that $S_\nu(t)$ is a direct measure of what one means by the "solvation response". This is the case if the probe solute is responsive only to the energetics of solute−solvent interactions and not to other processes such as relaxation among internal (vibrational and/or electronic) states. In the present work, we focus on the solute coumarin 153 (hereafter referred to as C153), which we have shown is an excellent probe of solvation.

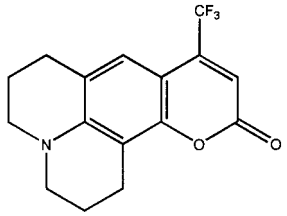

Coumarin 153

For example, the equilibrium spectral properties of C153 are highly correlated to the well-known $E_T(30)$ and π^* empirical polarity scales.[24] Simple dielectric solvation models closely approximate the dynamical response measured by the time-dependent fluorescence Stokes shift of C153 in a wide range of polar solvents.[21,25] Evidence from equilibrium and time-resolved data indicates that the magnitude of the dynamic Stokes shift of C153 is a direct measure of its interactions with the permanent charge moments of solvent molecules.[24] In other words, C153 is an ideal solvation probe.[26]

To measure $S_\nu(t)$ using a probe such as C153, time-resolved emission spectra recorded on an ultrafast time scale are required. To achieve high time resolution (typically using fluorescence upconversion), time-evolving spectra are reconstructed from emission transients recorded at a series of wavelengths spanning the steady-state emission band. This method, which has been employed in our past work,[20,21,24] is referred to as *spectral reconstruction*. Spectral reconstruction is completely general in that it makes no assumptions about the underlying photophysics

* To whom correspondence should be addressed. Tel.: (814) 865-0898. Fax: (814) 863-5319. E-mail: mpm@chem.psu.edu.

10.1021/jp984004q CCC: $18.00
Published on Web 02/11/1999

or photochemistry of the probe or the nature of the solvation process. But reconstructing spectra from emission transients is expensive and time consuming in terms of the effort required to collect the data and generate complete time-resolved spectra.

As a time-saving alternative, Barbara and co-workers proposed what they called the *single-wavelength method*.[27,28] This clever approach relies on a simple photodynamic model of a solvating probe[29] in order to approximate $S_\nu(t)$ from a single emission transient collected at a special linear-emission wavelength. This linear wavelength, which is specific to the solvatochromic probe employed, is identified through measurement of several photophysical properties. Using a variety of coumarins including C153, Barbara and co-workers demonstrated that the solvation-response functions produced by the single-wavelength approximation are similar to those obtained via the spectral-reconstruction method in a limited number of solvents.[22,23,28]

The purpose of the present paper is to examine the accuracy of the single-wavelength method in more detail. The extensive library of time-resolved and steady-state spectra of the solute C153 at our disposal enables a more definitive test of the method than has previously been possible. We compare solvation-response functions of C153 generated via the spectral-reconstruction and single-wavelength techniques in a set of 24 room-temperature solvents whose polarities and solvation times cover wide ranges. After briefly reviewing the spectral-reconstruction method, the basic theory and important assumptions underlying the single-wavelength approximation are described in some detail. Application of the single-wavelength method is then discussed specifically for the case of C153, and the optimal linear-emission wavelengths for monitoring the dynamics are identified. Solvation-response functions based upon two emission wavelengths are compared to equivalent response functions generated using the spectral reconstruction method. Corrections for nonlinear behavior of the spectral densities are also applied in an attempt to improve agreement between the linear-wavelength and spectral-reconstruction methods.

II. The Spectral-Reconstruction Method

The method of spectral reconstruction and its application to the study of solvation dynamics as monitored by C153 has been discussed at length in ref 21 and will not be repeated here. In brief, the steps used to transform a series of fluorescence up-conversion decays collected at 10−12 wavelengths into a spectral response function $S_\nu(t)$ are the following: (i) First, the emission transients are independently fit to multiexponential functions of time using an iterative reconvolution scheme. This process provides a convenient representation of the data and partially removes the influence of instrumental broadening. (ii) The intensities of the fitted transients are normalized relative to the steady-state spectrum in order to account for wavelength-dependent instrument responsivity (efficiency of the detector and sum frequency generation). The set of fitted transients then provides coarse spectra consisting of 10−12 frequency points at any desired time. (iii) These spectra are fit to a log-normal line-shape function in order to provide a continuous representation of the spectral dynamics. Examples of such spectra and their log-normal fits are displayed in Figure 1 for C153 in propylene carbonate solvent. (iv) $S_\nu(t)$ is finally derived from a combination of two measures of the spectral frequencies, the peak and the average (first-moment) frequencies, used in conjunction with estimates of these frequencies at infinite time (from steady-state spectra) and at zero time (using the method described in ref 30). The resulting $S_\nu(t)$ for 27 solvents are summarized in ref 21 (Table 3) and ref 24 (Table 4) in terms of multiexponential fits. These results are compared to new results obtained via the linear-wavelength approach in the present work.

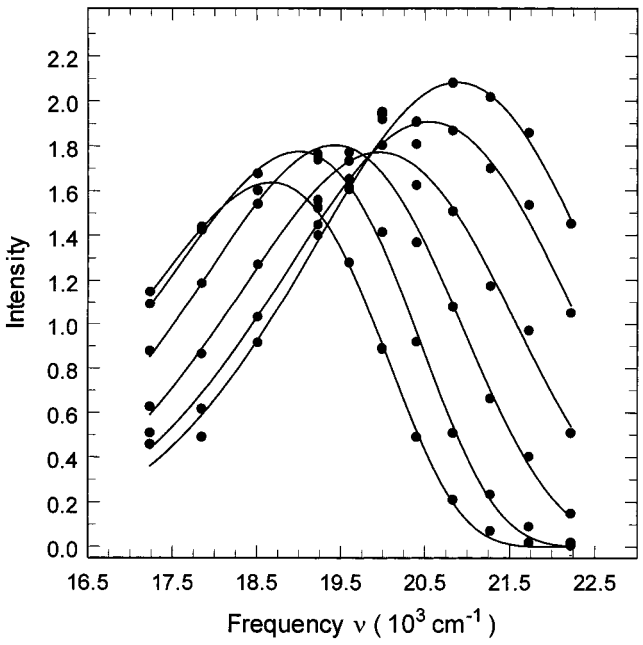

Figure 1. Time-resolved emission spectra of coumarin 153 in propylene carbonate. The "raw" spectra (open circles) and log-normal fits to the spectra (lines) are displayed at six times (0, 0.05, 0.2, 1, 5, and 200 ps).

III. The Single-Wavelength Method: Theory

The "single-wavelength" method, devised by Barbara and co-workers,[27,28] uses data collected under equilibrium solvation conditions along with emission decays measured at a single, special wavelength to approximate the spectral-response function. To derive the working equations of this method, we employ a slightly different notation from that of Barbara and co-workers, but the essential ideas are the same as expressed in their original work.[27] First, one adopts a one-dimensional "photodynamic" model[29] of the spectral effects of solvation. The photodynamic model assumes that a single polarization or solvation coordinate "z" is capable of completely describing how the interactions between the solute and its solvent surroundings affect its emission spectrum. Any time-dependence of the solute's photophysical properties derives solely from the time-evolution of the distribution of solvation states, $\rho(z,t)$. In particular, the time-dependent emission at any frequency, $D(\nu,t)$, can be written

$$D(\nu,t) \propto N(t) \int \mathrm{d}z \rho(z,t) g_{\mathrm{em}}(z,\nu) k_{\mathrm{rad}}(z) \qquad (2)$$

where $N(t)$ is the total excited-state population, $g_{\mathrm{em}}(z,\nu)$ is the emission line-shape function, and $k_{\mathrm{rad}}(z)$ is the radiative rate constant of a molecule in solvation state z. The excited-state population decay also involves a convolution over z

$$N(t) = N(0) \exp\{-\int_0^t \mathrm{d}t' \int \mathrm{d}z \rho(z,t') k_{\mathrm{tot}}(z)\} \qquad (3)$$

where k_{tot} is the total decay constant (radiative plus nonradiative components) of the excited state.

In addition to this one-dimensional perspective, the main assumption of the single-wavelength approach is that $\rho(z,t)$ can be approximated by some equilibrium distribution function $\rho_{\mathrm{eq}}^{(\pi)}(z)$, which represents the distribution of solvation states

observed under equilibrium conditions in a solvent of the appropriate polarity, "π". This polarity is defined such that the average value of z in the equilibrium solvent is the same as the instantaneous average of $\rho(z,t)$, denoted $\bar{z}(t)$. That is, one assumes

$$\rho(z,t) \cong \rho_{eq}^{(\pi)}(z); \quad \pi = \pi[\bar{z}(t)] \tag{4}$$

Since the average polarization in equilibrium depends on solvent polarity, the idea is that the temporal evolution of $\bar{z}(t)$, and thus the emission spectrum during dynamic solvation in a single solvent, is equivalent to the evolution of $\rho_{eq}^{(\pi)}(z)$ and the equilibrium spectrum as a function of solvent polarity π.

There is both experimental[1,21] and computational[31,32,33] evidence that suggests that $\rho(z,t)$ does not actually evolve through intermediate equilibrium distributions in such a simple manner. For example, the spectral width actually tends to go through a maximum as a function of time, while the equilibrium spectra narrow monotonically as a function of increasing solvent polarity (compare Figures 11 and 15 of ref 21). However, because the vibronic contribution typically dominates the width of the emission spectrum, changes in the width and shape of the time-evolving spectra are relatively minor effects compared to the frequency shift. The above approximation is therefore not unreasonable. It allows $D(\nu,t)$ to be expressed as

$$D(\nu,t) \propto G_{em}^{eq}(\bar{\nu}(t);\nu)K_{rad}^{eq}(\bar{\nu}(t)) \exp\{-\int_0^t dt' K_{tot}^{eq}(\bar{\nu}(t'))\} \tag{5}$$

The functions G_{em}^{eq}, K_{rad}^{eq}, and K_{tot}^{eq} here differ from their "microscopic" counterparts g_{em}, k_{rad}, and k_{tot} in that they are averaged over an equilibrium distribution of solvation environments. For example,

$$K_{rad}^{eq}(\pi) = \int dz \rho_{eq}^{(\pi)}(z) k_{rad}(z) \tag{6}$$

The notation $K_{rad}^{eq}(\bar{\nu}(t))$ etc. in eq 4 derives from measuring solvent polarity "π" in terms of the average frequency of the emission spectrum of the solute in question, $\bar{\nu}$. Thus, $K_{rad}^{eq}(\bar{\nu}(t))$ denotes the value of the radiative rate that would be measured under equilibrium solvation conditions in a solvent for which the frequency of the (equilibrated) emission spectrum is equal to the instantaneous frequency $\bar{\nu}(t)$ of the time-evolving spectrum at a given time t.

Convenient application of the single-wavelength method requires that one further simplification be made to the exponential decay term in eq 5. In most systems of interest, solvation dynamics are much faster than population decay. For such cases it is appropriate to ignore the time-dependence of $K_{tot}^{eq}(\bar{\nu}(t))$ and approximate the exponential term by the value observed at long times, $\exp\{-K_{tot}^{\infty}\}$ with $K_{tot}^{\infty} \equiv K_{tot}^{eq}[\bar{\nu}(\infty)]$. Then the renormalized emission decay, $D'(\nu,t)$, can finally be cast in the form

$$D'(\nu,t) \equiv D(\nu,t) \exp\{+K_{tot}^{\infty} t\} \propto G_{em}^{eq}(\bar{\nu}(t);\nu)K_{rad}^{eq}(\bar{\nu}(t)) \tag{7}$$

This expression shows that for any emission frequency, ν, $D'(\nu,t)$ is related to the time evolution of the average frequency $\bar{\nu}(t)$ through the "spectral density" function

$$\psi(\bar{\nu}) \equiv G_{em}^{eq}(\bar{\nu};\nu)K_{rad}^{eq}(\bar{\nu}) \tag{8}$$

which can be measured under equilibrium solvent conditions.

The simplest application of the single-wavelength method relies upon finding a specific observation wavelength or frequency ν_{LW} such that the spectral density is linearly related to the average frequency

$$\psi(\bar{\nu}) \cong a_1 + a_2\bar{\nu} \tag{9}$$

In this case, the emission transient at ν_{LW} can be used to approximate $S_\nu(t)$ via

$$S_{LW}(t) \equiv \frac{D'(\nu_{LW},t) - D'(\nu_{LW},\infty)}{D'(\nu_{LW},0) - D'(\nu_{LW},\infty)} \cong \frac{\bar{\nu}(t) - \bar{\nu}(\infty)}{\bar{\nu}(0) - \bar{\nu}(\infty)} \equiv S_\nu(t) \tag{10}$$

Although applications of the single-wavelength method made to date have employed eq 10, there is nothing that precludes application of the formalism in cases where the linear condition, eq 9, is not satisfied. In principle, any observation wavelength can be used, provided that the relationship between $\psi(\bar{\nu})$ and $\bar{\nu}$ can be represented by a simple monotonic function. In this case, one merely inverts the function to determine the average frequency of the time-evolving spectrum via

$$\bar{\nu}(t) \cong \psi^{-1}[D''(\nu,t)] \tag{11}$$

and approximates the normalized response function by

$$S_{NL}(t) \equiv \frac{\psi^{-1}[D''(\nu,t)] - \psi^{-1}[D''(\nu,\infty)]}{\psi^{-1}[D''(\nu,0)] - \psi^{-1}[D''(\nu,\infty)]} \cong S_\nu(t) \tag{12}$$

The subscript "NL" is used to distinguish this more general, "nonlinear" single-wavelength approach from its linear approximation, eq 10. (The difference between $D'(\nu,t)$ and $D''(\nu,t)$ involves an additional normalization step, eq 15, which is discussed in the following section.)

IV. The Single-Wavelength Method: Application to Coumarin 153

Application of the simplest version of the single-wavelength approach requires identification of a special frequency, ν_{LW}, for which the spectral-density function $\psi(\bar{\nu})$ is linear in the average-emission frequency $\bar{\nu}$. To determine $\psi(\bar{\nu})$, equilibrated emission spectra and radiative rates are required in a collection of solvents whose average frequencies span the range of dynamical shifts $\bar{\nu}(t)$ expected. To obtain such data, two approximations are made here: (i) that the steady-state emission spectra in most solvents provide a good representation of $G_{em}^{eq}(\bar{\nu};\nu)$ and (ii) that the radiative rates of C153 are simply proportional to the cube of the average emission frequency

$$K_{rad}^{eq}(\bar{\nu}) \propto \bar{\nu}^3 \tag{13}$$

The first of these approximations should be valid for C153 in nearly all solvents at room temperature. Although the steady-state emission spectrum strictly reflects a time integral over all instantaneous emission spectra, given the speed of solvation (t_{1e} < 10 ps in most cases) compared to the emission lifetime (4−6 ns), the steady-state emission is dominated by contributions from equilibrated solvation states. The second approximation eliminates the need to measure the radiative rates in all solvents. In a recent study of the solvent dependence of transition moments,[34] eq 13 was found to hold for the case of C153 to better than 10% in a collection of 12 solvents having widely different polarities and other characteristics.[35] It will be assumed here for convenience.

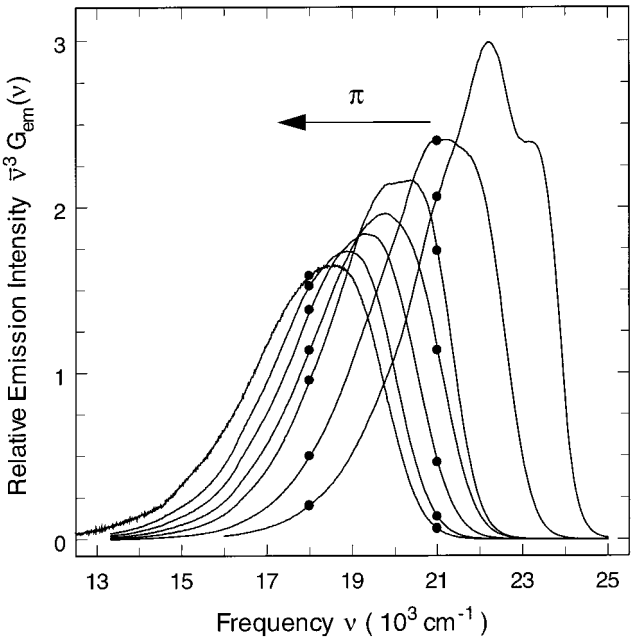

Figure 2. Representative emission spectra of C153 in a series of solvents. The solvents are from right to left: cyclohexane, diethyl ether, chloroform, methyl acetate, acetone, dimethylformamide, and propylene carbonate. Emission intensities at 18 000 cm^{-1} and 21 000 cm^{-1} are highlighted to illustrate the behavior of the spectral density in various solvents.

Scaled emission spectra ($\bar{\nu}^3 G_{em}(\nu)$) of the sort used to determine the spectral density function are displayed in Figure 2. (Details of the procedures employed in obtaining the steady-state emission spectra and a complete listing of solvents and spectral characteristics are found in ref 24.) As the solvent polarity increases from cyclohexane to propylene carbonate, the scaled spectra shift to the red and decrease in intensity as a result of the solvent dependence of the radiative rate. The points emphasized in Figure 2 illustrate the meaning of the spectral density function observed at two different frequencies, $\nu =$ 18 000 and 21 000 cm^{-1}. Each vertical set of points corresponds to seven ($\bar{\nu},\psi$) pairs from the spectral-density function $\psi(\bar{\nu})$ for that observation frequency. A ($\bar{\nu},\psi$) point is simply defined by the first moment frequency $\bar{\nu}$ of the spectrum and the intensity ψ (at the particular observation frequency ν) read off of one of these suitably normalized emission spectra. Although only seven spectra are illustrated here for clarity, spectral densities in this work were measured using data recorded for a total of 36 room-temperature solvents. This solvent collection includes dipolar aprotic, nondipolar, and hydrogen bonding solvents, which encompass a wide range of polarity and other characteristics (see ref 24).

Before examining the spectral densities further, it is interesting to note the similarity between the scaled equilibrium spectra in Figure 2 and the time-evolving spectra shown in Figure 1. Normalizing the long-time spectrum ($t = 200$ ps) from Figure 1 to the $\bar{\nu}^3$-weighted equilibrium spectrum of propylene carbonate, one obtains the comparison shown in Figure 3. The qualitative agreement between the steady-state and time-evolving spectra is typical of what is seen in many solvents. It generally supports the assumption that the time-evolving spectra can be approximated by spectra observed in equilibrium. However, the agreement is far from perfect. The relative intensities and shapes/widths of the two types of spectra differ quantitatively. In general, the width of the time-zero spectrum tends to be narrower than that of the corresponding equilibrium spectrum, while at intermediate times the time-evolving spectrum is broader than the equilibrium spectrum. The effects of these differences will be discussed later.

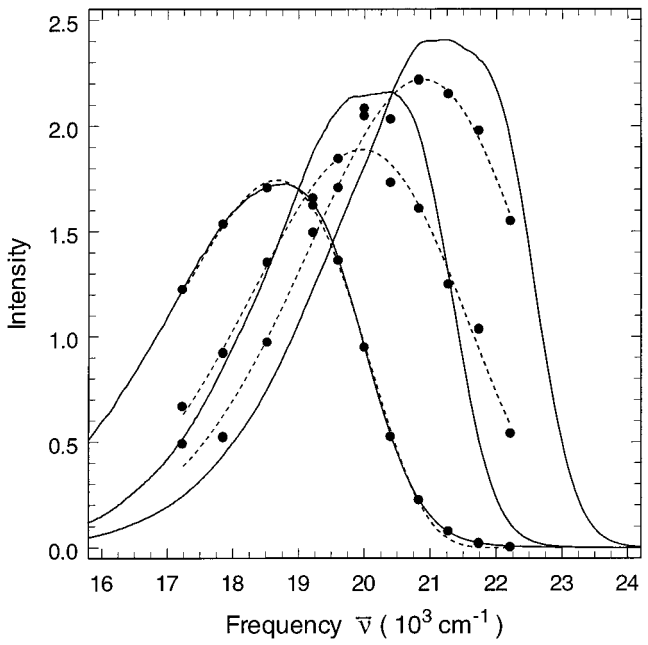

Figure 3. Comparison of time-evolving and equilibrium spectra. Time-resolved spectra (broken lines and symbols) at 0.0, 0.2, and 200 ps are compared to $\bar{\nu}^3$ weighted equilibrium spectra (solid lines) in the solvents diethyl ether, methyl acetate, and propylene carbonate, respectively. The two sets of spectra have been relatively normalized to equal intensity for the 200-ps steady-state spectrum in propylene carbonate.

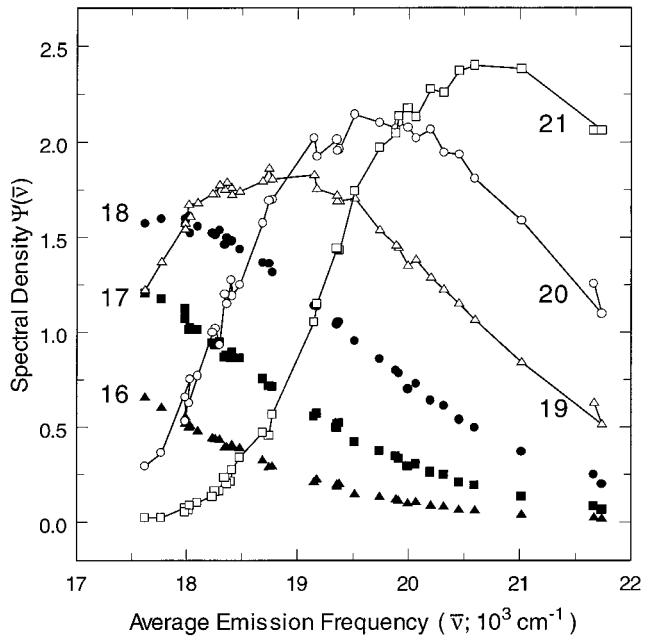

Figure 4. Solvent dependence of the spectral-density function. Spectral densities of C153 are plotted as a function of solvent polarity at six emission frequencies. For clarity, emission frequencies (16,000−18,000 cm^{-1}) on the red edge are designated as solid symbols while the frequencies on the blue edge (19,000−21,000 cm^{-1}) are shown as open symbols.

The dependence of the spectral density $\psi(\bar{\nu})$ on the average emission frequency $\bar{\nu}$ is shown for six different observation frequencies in Figure 4. Several things are remarkable about these data. First, despite experimental uncertainties, the individual spectral-density functions show relatively little scatter. Their smooth appearance supports the idea that a single variable such as solvent polarity simultaneously controls all of the

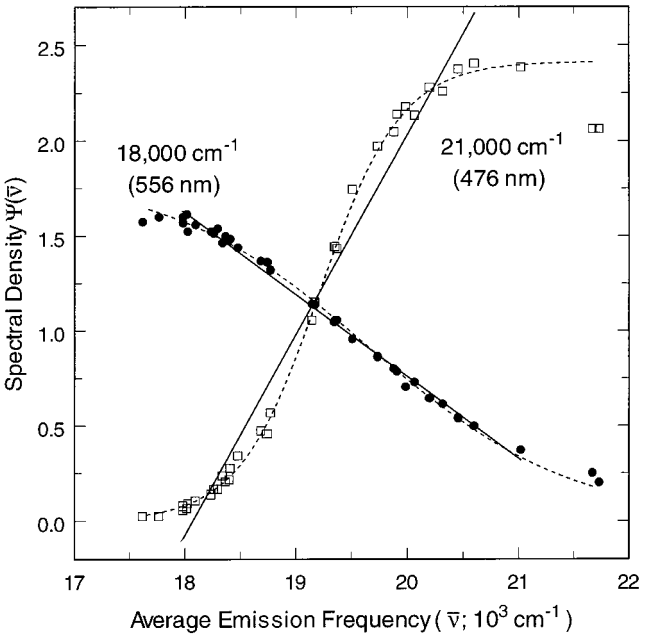

Figure 5. Spectral-density functions at emission frequencies 18 000 cm^{-1} and 21 000 cm^{-1}. Solid lines represent linear fits to the spectral densities while the dashed lines represent nonlinear fits to eq 14. Parameters of the linear and nonlinear fits are provided in Table 1.

features of the equilibrium emission of C153 (i.e., its position, width, and intensity) in all solvents. The spectral densities show a systematic progression from the red to the blue side of the spectrum. At observation frequencies less than 17 000 cm^{-1}, $\psi(\bar{\nu})$ decreases monotonically with increasing $\bar{\nu}$. For very blue observation frequencies (ν>21 000 cm^{-1}, not shown), $\psi(\bar{\nu})$ monotonically increases with $\bar{\nu}$, and for intermediate frequencies the spectral density goes through a maximum. This behavior is reminiscent of the behavior observed at different frequencies in the time-evolving spectra. (Compare, for example, the time dependence of the intensities of the spectra in Figure 1 at frequencies of 18 000, 19 000, and 21 500 cm^{-1} to the $\bar{\nu}$ dependence of the spectral density functions at these observation frequencies.) The final noteworthy feature of the data in Figure 4 is that there is no observation frequency for which $\psi(\bar{\nu})$ is a truly linear function of $\bar{\nu}$ over the entire frequency range studied.

Fortunately, application of the linear-wavelength method only requires approximate linearity of $\psi(\bar{\nu})$ over the range of frequencies likely to be encountered in a particular time-evolving spectrum, typically between 17 000−21 000 cm^{-1} for C153. On the basis of data such as those shown in Figure 4 and similar data at intermediate frequencies, the two best candidates for linear-observation frequencies were determined to be 18 000 cm^{-1} (556 nm) and 21 000 cm^{-1} (476 nm). Linear (solid lines) and nonlinear (dashed curves) fits to these spectral densities are shown in Figure 5, and the parameters characterizing these fits are summarized in Table 1. The nonlinear fits employ the function

$$\psi(\bar{\nu}) = \frac{a_1}{1 + \exp(-(\bar{\nu} - a_2)/a_3)} \tag{14}$$

which was chosen because it can be analytically inverted for use in eq 11.

Two observations can be made from the fits illustrated in Figure 5. First, it would appear that 556 nm is the better choice of linear wavelength. Over the most important range, $\psi(\bar{\nu})$ departs only slightly from linearity, whereas in the case of 476-nm data, the deviations are much larger. We note that in their original work with a more limited set of solvents, Barbara and co-workers selected 480 nm as the linear wavelength for C153,[23] close to the 476-nm value obtained in the present work. However, they did not mention the possibility of another wavelength on the red side of the spectrum. The second feature evident from these fits is that even at 556 nm, the spectral densities are not truly linear in $\bar{\nu}$. As indicated by the results in Table 1, a sigmoidal representation of the data according to eq 14 provides a significantly improved fit.

TABLE 1: Summary of Fit Parameters to Spectral Densities[a]

	linear fit		nonlinear fit	
	476 nm	556 nm	470 nm	560 nm
a_1	19.06	9.41	2.52	1.81
a_2	1.05	−0.43	19.50	19.50
a_3			0.388	−0.942
$\bar{\nu}$ range fit	18.1−20.5	18.1−21.0	17.6−21.0	17.6−21.0
no. of solvents	26	28	34	34
correlation coefficient	0.976	0.993	0.999	0.998

[a] a_1−a_3 refer to the parameters of eqs 9 (linear) at 14 (nonlinear). Only a subset of the complete data set was fit in each case. The number of solvents and $\bar{\nu}$ range spanned by the data are indicated.

On the basis of these observations, one would conclude that the linear-wavelength approximation is best applied to data collected at 556 nm. In addition, the nonlinear version of the single-wavelength method should improve the predictions made at both emission wavelengths, but especially those measured at 476 nm. However, it must be remembered that the single-wavelength approach rests on a model of the spectral evolution that is not exact (see Figure 3). Conclusions regarding how best to apply the method should therefore not be made on the basis of the spectral densities alone. One must examine the quality of the dynamical predictions themselves before making any final judgment. For this reason, the dynamical predictions made using both the linear and nonlinear versions of the single-wavelength method at both observation wavelengths will be examined.

Before presenting these comparisons, a few additional comments concerning determination of the single-wavelength response functions are necessary. First, since the data employed here were obtained previously, we do not have data at precisely the wavelengths 476 and 556 nm. Instead we use the closest available wavelengths, which are 470 and 560 nm.[36] $S_{LW}(t)$ functions are determined from time-resolved data at these wavelengths by first deconvoluting the instrument response from the data, multiplying by the population factor $\exp\{-K_{tot}^{\infty}\}$ to obtain $D'(\nu,t)$ and, finally, applying eq 10. To construct $S_{NL}(t)$, one further piece of information is required. Since the spectral densities depend on frequency in a nonlinear manner, it is necessary to have a well-defined intensity reference. For this purpose, the emission decay, $D'(\nu,t)$, is normalized to match the spectral density function at time infinity

$$D''(\nu,t) = \frac{\psi(\bar{\nu},t=\infty)}{D'(\nu,t=\infty)} D'(\nu,t) \tag{15}$$

This normalization scheme works well for the 560-nm data because the emission increases with time such that there is sufficient intensity at long times to accurately normalize the decay. However, at 470 nm, the emission transients decay rapidly, leaving little intensity available at "$t = \infty$" with which

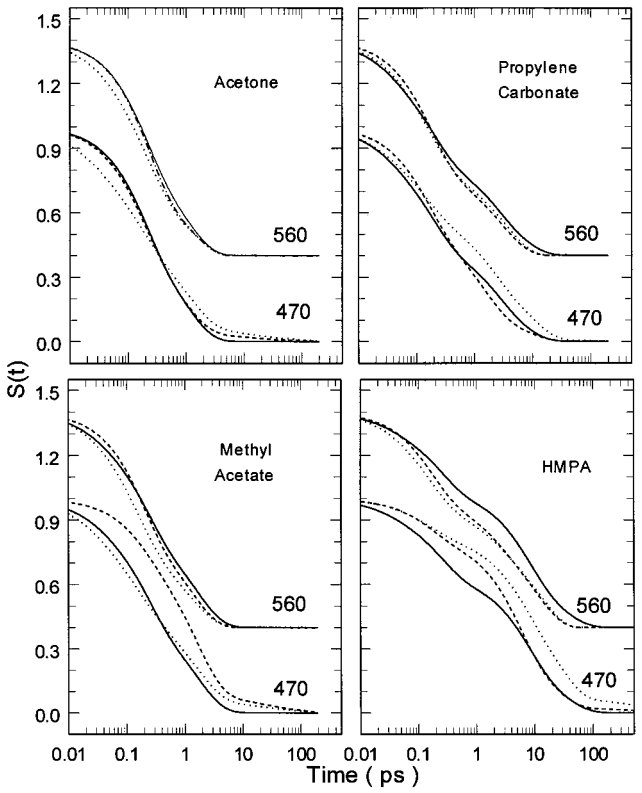

Figure 6. Representative spectral-response functions estimated using the linear and nonlinear versions of the single-wavelength method. The solvation-response functions, $S_\nu(t)$ (solid), $S_{LW}(t)$ (long dash), and $S_{NL}(t)$ (short dash) are displayed for the solvents acetone, propylene carbonate, methyl acetate, and HMPA. Solvation-response functions based upon 560-nm data are vertically offset for clarity.

to accurately normalize the data in many of the solvents surveyed. As a result, estimates of the time-zero frequency are used to normalize the 470-nm data. Since it has been demonstrated that the time-zero estimates[30] accurately predict the time-zero frequency observed in experiment,[21] this further approximation is believed to contribute little to the error of the method. A final detail of the analysis procedure results from the fact that the $S_\nu(t)$ data reported in ref 21 represent a weighted average of several independently collected data sets for each solvent. Relative weights assigned to the individual $S_\nu(t)$ were based on several factors that included the appearance of the time-resolved spectra and time resolution on a given day. In generating single-wavelength results, this same averaging scheme was applied in order to provide the most accurate comparison between the two methods.

V. Comparison of Solvation-Response Functions

Representative spectral-response functions obtained via spectral reconstruction ($S_\nu(t)$) are compared to all four of the single-wavelength approximations, $S_{LW}^{470}(t)$, $S_{LW}^{560}(t)$, $S_{NL}^{470}(t)$, and $S_{NL}^{560}(t)$ in Figure 6. The level of agreement between $S_\nu(t)$ and these various approximations, displayed here in four selected solvents, is typical of what is observed in all of the cases studied. In many instances both the shape and time scales of $S_\nu(t)$ are nicely captured by the single-wavelength predictions. However, in other instances, especially at the 470-nm observation wavelength, the predictions are in substantial error.

The predictions of the linear single-wavelength method, $S_{LW}^{470}(t)$ and $S_{LW}^{560}(t)$, will be examined first. One simple measure of the agreement between these response functions and $S_\nu(t)$ is obtained by comparing their respective $1/e$ times, t_{1e}. This

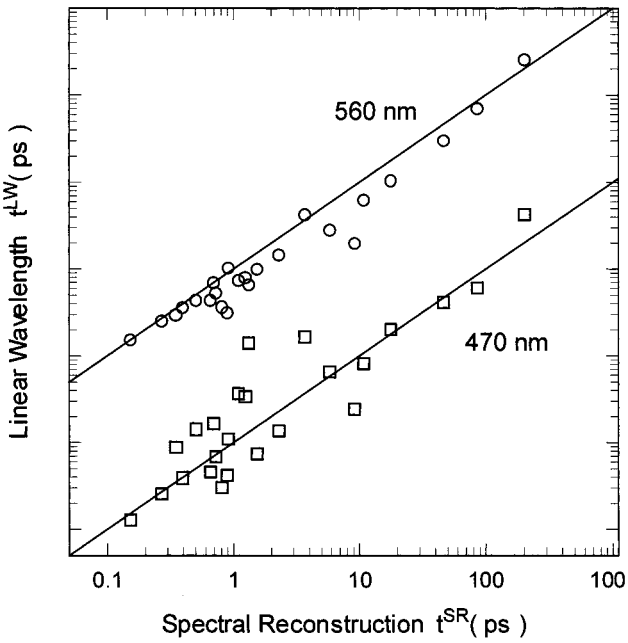

Figure 7. Comparison of 1/e times obtained from the linear single-wavelength approximation and from spectral reconstruction. Results obtained using 470- and 560-nm observation wavelength have been offset for clarity. The lines represent agreement between the linear wavelengths and spectral-reconstruction times.

characteristic, defined as the time required for $S(t)$ to relax to a value of $1/e$ (0.368), is compiled for each of the response functions in Table 2. In Figure 7, t_{1e}^{470} (squares) and t_{1e}^{560} (circles) derived from $S_{LW}(t)$ are plotted against t_{1e}^{SR} from $S_\nu(t)$. The lines represent agreement between the times obtained from the two methods. The results displayed in Figure 7 demonstrate that the linear-wavelength method captures the basic time scale of the $S_\nu(t)$ response in a wide range of solvents whose solvation times differ by more than a factor of 1000. However, one also observes significant scatter about the lines and an apparent systematic deviation in the case of the 560-nm predictions.

To quantify the level of agreement between these times, logarithmic ratios defined by

$$R_{1e}(\alpha) = \log_{10}\left[\frac{t_{1e}^{\lambda}(\alpha)}{t_{1e}^{SR}(\alpha)}\right] \tag{16}$$

are used (α is a solvent index). These ratios for both t_{1e}^{470} and t_{1e}^{560} are displayed as functions of the solvation time t_{1e}^{SR} in Figure 8. Note that a positive value of R_{1e} indicates $S_{LW}(t)$ achieves the same amount of solvent relaxation in more time than $S_\nu(t)$, or in other words, that $S_{LW}(t)$ reports a slower response than $S_\nu(t)$. The dashed lines in this and subsequent figures indicate agreement to within a factor of 1.4 (short dash) and 2.0 (long dash). (The value of 1.4 is chosen because it is approximately twice the estimated error in the spectral reconstruction results.[37]) In the case of the 470-nm data, the values of $R_{1e}^{470}(\alpha)$ are randomly distributed with respect to solvation time, but the scatter of the data is considerable. Only half of the linear-wavelength times are within a factor of 2 of the spectral-reconstruction times. In contrast, for the 560-nm observation wavelength, the majority of the data (20/24 solvents) are within a factor of 2 of t_{1e}^{SR}. However, the average value of $R_{1e}^{560}(\alpha)$ is not zero but -0.18, indicating that the linear-wavelength predictions made at 560 nm are, on average, a factor of 1.5 less than the spectral-reconstruction times. Finally, there

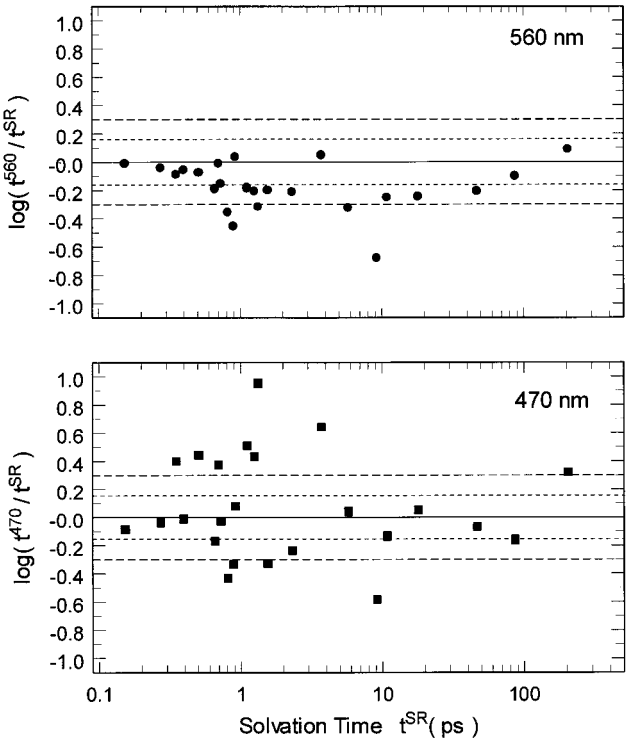

Figure 8. Logarithmic ratios of 1/e times (R_{1e}; eq 16) estimated via the linear-wavelength method at 470- and 560-nm emission wavelengths and spectral-reconstruction results plotted against spectral-reconstruction times. The solid line represents agreement between t_{1e}^{SR} and $t_{1e}^{1\lambda}$, while the short and long dashed lines mark log values of ± 0.16 and ± 0.30 corresponding to factors of 1.4 and 2.0, respectively.

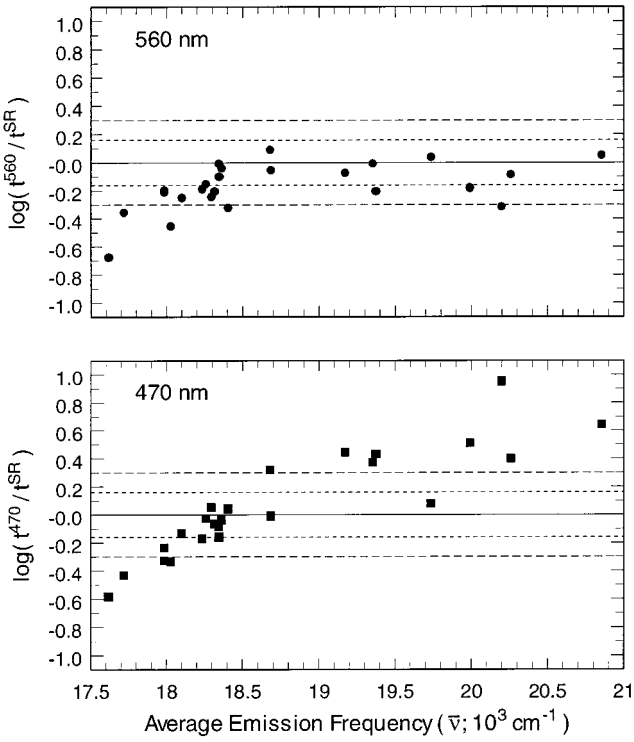

Figure 9. Logarithmic ratios of 1/e times (R_{1e}; eq 16) estimated via the linear-wavelength method at 470- and 560-nm emission wavelengths and spectral-reconstruction results plotted against the average steady-state emission frequency ($\bar{\nu} = \nu(t = \infty)$).

are no obvious trends at either observation wavelength with solvation time or solvent type.

There are, however, trends in the quality of the linear-wavelength predictions when viewed as a function of average steady-state emission frequency ($\bar{\nu} = \nu(\infty)$), as is illustrated in Figure 9. In the case of the 470-nm data, the predicted times progress from being much too fast at low $\bar{\nu}$ to being much too slow at large $\bar{\nu}$. In the case of the 560-nm data, the trend is not as dramatic, but it is clear that the poorest agreement with t_{1e}^{SR} is obtained for solvents with the lowest values of $\bar{\nu}$. While the deviations displayed here are not causally linked to solvent polarity, the high and low values of $\bar{\nu}$ correspond to solvents with high and low polarities, respectively.

An understanding of the source of the errors in the linear-wavelength predictions can be obtained by examining the deviations from linearity of the spectral densities shown in Figure 5. In the linear-wavelength approach, the transformation between intensity (D' or ψ) and frequency ($\bar{\nu}$) is assumed to be such that $d\psi/d\bar{\nu}$ is constant over the range of frequencies sampled during the spectral evolution. The method fails primarily when there is a substantial change in this slope over the relevant frequency range. In the case of the 470-nm observation wavelength, there is strong curvature in $\psi(\bar{\nu})$ at both low and high $\bar{\nu}$, whereas in the case of 560-nm important curvature mainly occurs on the low-frequency end. Thus, there is a correlation between curvature in $\psi(\bar{\nu})$ and the magnitude of the errors in the times predicted by the linear-wavelength approach. In addition, the sign of the error is what one would expect based on the results of simple model calculations. For single exponential $\nu(t)$ and constant curvature, one finds that the linear approximation underestimates the speed of the true $\nu(t)$ dynamics when the curvature is such that $d\psi/d\bar{\nu}$ is greatest at long times (small $\bar{\nu}$) and likewise overestimates the speed when $d\psi/d\bar{\nu}$ is smallest at short times. This behavior is precisely what is observed in the experimental data.

The above analysis suggests that application of the more general, nonlinear version of the single-wavelength method should significantly improve its accuracy. Unfortunately, this is not the case. As illustrated by the response functions in Figure 6, there are often substantial differences between the linear (dashed) and nonlinear (dotted curves) single-wavelength predictions, especially for emission at 470 nm. The only systematic distinction between $S_{LW}(t)$ and $S_{NL}(t)$ is that the initial decay of $S_{NL}(t)$ tends to be faster than that of $S_{LW}(t)$. In some cases, $S_{NL}(t)$ is in better agreement with $S_\nu(t)$ than $S_{LW}(t)$, but in just as many cases it is not.

Figure 10 compares the 1/e times of the $S_{NL}(t)$ and $S_\nu(t)$ decays in the form of logarithmic ratios (solid symbols). Also shown for comparison are the linear-wavelength results from Figure 9 (open symbols). The relationship between the nonlinear and linear predictions is what one would expect based on the discussion presented above. That is, solvents whose average dynamical frequencies fall below the inflection points of the spectral-density curves (a_2 of the nonlinear fits in Table 1) are shifted toward slower times compared to the linear predictions, whereas those at higher frequencies are shifted toward faster times. In the case of 560-nm emission, the nonlinear method provides improved agreement with the spectral reconstruction times for solvents falling in the low-frequency portion of the data, but for solvents whose spectral evolution occurs above 19 000 cm^{-1}, the agreement is poorer than with the linear method. For the 470-nm observation wavelength, the nonlinear method nearly always corrects the linear-wavelength predictions in the proper direction, but, at least in the solvents at the low frequency end of the data set, the correction badly overshoots the mark. The net result is that, at least based on the 1/*e* times, there is no clear improvement over the predictions of the linear wavelength method.

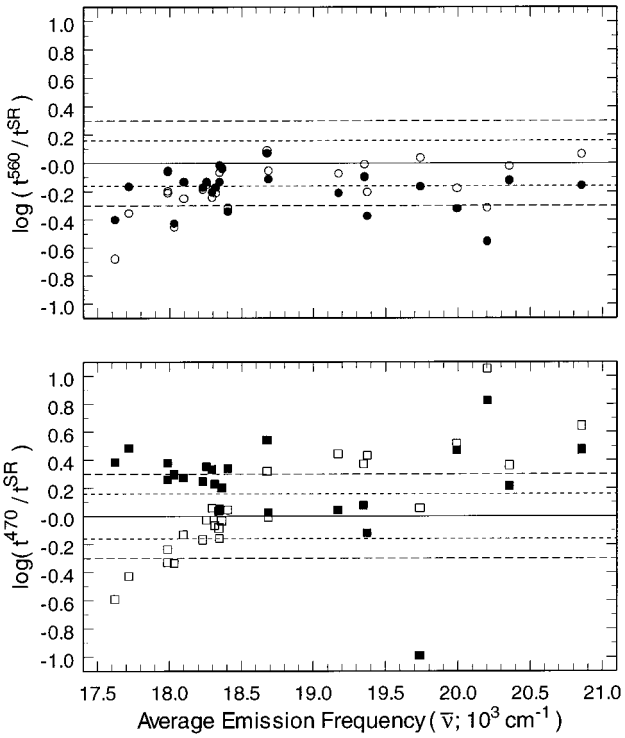

Figure 10. Comparison of logarithmic ratios estimated via the nonlinear (solid symbols) and linear (open symbols) single-wavelength methods at 470 and 560 nm.

VI. Calibration and Recommendations for the Use of the Single-Wavelength Method

To more completely assess the relative accuracy of the various methods, it is important to examine more than only the 1/*e* times. Since the solvation-response functions are usually at least biexponential functions of time, an overall evaluation should in some way acknowledge the dispersive character of the dynamics. To this end, logarithmic ratios such as those defined in eq 16 were calculated from the times required to reach eight distinct levels of relaxation, $S(t) = 0.1, 0.2, ..., 0.8$. Figure 11 shows these ratios at four different relaxation levels for the linear 560-nm response functions. One observes a consistent pattern of errors at all $S_\nu(t)$ levels in these data. Similar behavior is also observed for the other single-wavelength methods. This consistency reflects the fact that $S_{1\lambda}(t)$ usually is found to be uniformly faster or slower than $S_\nu(t)$ in a given solvent, and thus the pattern of *R* values is largely maintained for different relaxation levels and is comparable to that displayed for 1/*e* times. But, as shown in Figure 6, there are also examples in which the predicted and observed $S_\nu(t)$ decays cross. For this reason it seems most appropriate to incorporate all of these data in a complete comparison of $S_{1\lambda}(t)$ and $S_\nu(t)$. For a given solvent α, the average absolute ratio

$$\langle |R(\alpha)| \rangle \equiv {}^1/_8 \sum_{\substack{i=1 \\ \text{level}}}^{8} |R_i(\alpha)| \tag{17}$$

serves to quantify the fit over all times. The average *R* values obtained in this manner are listed in Table 2. They are typically close to the (unsigned) *R* values defined in terms of 1/*e* times and displayed in Figures 8−10.

To compare the overall quality of the predictions of the different single-wavelength methods, two figures of merit are considered. The first simply involves counting the number of solvents (α) having $\langle |R| \rangle$ values within certain ranges. These numbers are listed in the rows labeled "no. of $\langle |R| \rangle$" in Table 3. Second, the entire solvent set is examined at these different relaxation levels by computing the overall unsigned and signed averages,

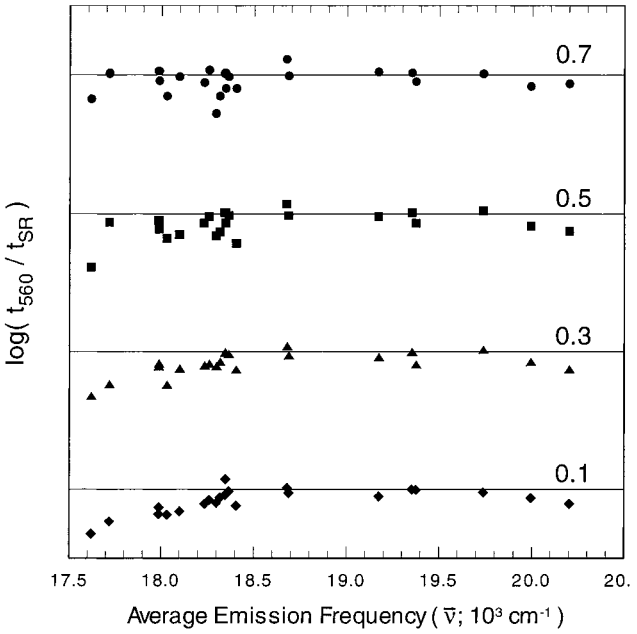

Figure 11. Logarithmic time ratios analogous to those defined in eq 16 for various levels of $S(t)$ relaxation ($S(t) = 0.1$, 03, 0.5, and 0.7, as indicated). These data are for the linear single-wavelength method using 560-nm observation wavelength. Lines indicate agreement between the times of $S_{LW}(t)$ and $S_\nu(t)$.

$$\langle\langle |R| \rangle\rangle = \frac{1}{24 \cdot 8} \sum_{\substack{\alpha=1 \\ \text{solvent}}}^{24} \sum_{\substack{i=1 \\ \text{level}}}^{8} |R_i(\alpha)| \tag{18}$$

and

$$\langle\langle R \rangle\rangle = \frac{1}{24 \cdot 8} \sum_{\substack{\alpha=1 \\ \text{solvent}}}^{24} \sum_{\substack{i=1 \\ \text{level}}}^{8} R_i(\alpha) \tag{19}$$

Values of these averages are also provided in Table 3.

As anticipated from the last section, the results compiled in Table 3 indicate that there is no significant improvement afforded by the nonlinear method. The average absolute deviations $\langle\langle |R| \rangle\rangle$ and the standard deviations in the signed *R* values do not change appreciably between the linear and nonlinear methods. In addition, significantly fewer solvents show the highest level of agreement ($\langle |R| \rangle < 0.1$) with the spectral-reconstruction results when the nonlinear method is used. Given this lack of improvement and the fact that the nonlinear method is more difficult to apply, the linear method is to be preferred. In addition, by all of the measures examined here, the predictions made using the 560-nm data are clearly superior to those made at 470 nm.

In conclusion, when using the single-wavelength method with the C153 probe, a 560-nm observation wavelength and use of the linear approximation is recommended. The signed averages in Table 3 are nonzero for this method. It is therefore also recommended that the results obtained in this way be modified to remove the average deviation by scaling the times so-obtained by a factor of 1.35. Application of such a time scaling for the current data set yields the results listed in the last column of

TABLE 2: Summary of Solvation Times obtained from the Spectral-Reconstruction and Linear-wavelength methods

	frequency[b] (10^3 cm^{-1})		1/e times (ps)					$\langle\|R(\alpha)\|\rangle$[d]			
solvent[a]	ν_0	ν_∞	t_{1e}^{SR}	t_{1e}^{470}	t_{1e}^{560}	t_{1e}^{470NL}	t_{1e}^{560NL}	470	560	470-NL	560-NL
butyl benzene	20.86	20.28	3.76	16.5	4.21	11.1	2.59	0.90	0.29	0.71	0.22
toluene	20.79	20.20	1.35	14.1	0.65	8.87	0.37	1.18	0.21	0.95	0.41
benzene	20.71	19.99	1.12	3.61	0.73	3.26	0.53	0.52	0.25	0.49	0.29
1,4-dioxane	20.98	19.74	0.92	1.09	1.01	0.09	0.63	0.23	0.02	0.81	0.16
dimethyl carbonate	20.89	19.36	1.26	3.37	0.78	0.95	0.53	0.43	0.13	0.26	0.27
tetrahydrofuran	20.66	19.35	0.71	1.65	0.69	0.84	0.56	0.34	0.02	0.11	0.09
methyl acetate	20.82	19.17	0.51	1.41	0.43	0.56	0.31	0.41	0.07	0.10	0.18
dichloromethane	20.36	19.15	0.38	0.88	0.36	0.63	0.29	0.33	0.02	0.16	0.11
acetone	20.53	18.69	0.40	0.39	0.35	0.42	0.31	0.02	0.04	0.16	0.13
1-decanol	20.75	18.68	205.	427.	251.	711.	239.	0.54	0.18	0.60	0.11
HMPA[a]	20.04	18.41	5.86	6.41	2.80	12.7	2.67	0.21	0.27	0.47	0.33
nitromethane	20.28	18.37	0.28	0.25	0.25	0.44	0.25	0.03	0.04	0.18	0.05
1-pentanol	20.42	18.35	87.1	59.9	69.1	97.9	83.6	0.13	0.13	0.04	0.16
acetonitrile	20.67	18.35	0.15	0.13	0.15	0.17	0.11	0.07	0.03	0.20	0.19
1-butanol	20.39	18.32	47.4	40.6	29.5	79.5	31.8	0.18	0.17	0.28	0.22
1-propanol	20.30	18.30	18.1	20.0	10.3	38.5	11.3	0.26	0.33	0.41	0.34
propylene carbonate	20.37	18.26	0.73	0.69	0.52	1.63	0.54	0.10	0.11	0.22	0.07
dimethylformamide	20.22	18.24	0.67	0.45	0.43	1.18	0.45	0.16	0.17	0.15	0.18
ethanol	20.33	18.10	10.9	7.96	6.13	20.4	8.05	0.19	0.29	0.31	0.15
dimethyl sulfoxide	20.05	18.03	0.90	0.41	0.31	1.77	0.33	0.31	0.38	0.19	0.38
methanol	20.46	17.99	2.33	1.34	1.42	5.51	2.06	0.18	0.17	0.30	0.12
N-methylformamide	20.18	17.99	1.57	0.73	0.99	2.83	1.36	0.21	0.17	0.26	0.11
ethylene glycol	19.79	17.62	9.29	2.41	1.94	22.4	3.67	0.45	0.59	0.45	0.37
formamide	19.74	17.72	0.82	0.30	0.36	2.46	0.56	0.32	0.25	0.45	0.17

[a] HMPA denotes hexamethylphosphoramide. [b] Time-zero and steady-state emission frequencies obtained from ref 24. [c] Solvents are ordered according to the steady-state emission frequency of C153, which is used as a measure of solvent polarity. [d] $\langle|R(\alpha)|\rangle$ denotes the average logarithmic ratios of times defined by eqs 16 and 17.

TABLE 3: Indicators of the Overall Accuracy of the Single-Wavelength Predictions

	linear 470	nonlinear 470	linear 560	nonlinear 560	scaled linear 560
no. of $\langle\|R\|\rangle \le 0.1$	3	1	7	3	8
no. of $\langle\|R\|\rangle \le 0.2$	9	8	15	15	19
no. of $\langle\|R\|\rangle \le 0.3$	13	13	21	19	21
no. of $\langle\|R\|\rangle > 0.3$	11	11	3	5	3
$\langle\langle\|R\|\rangle\rangle$	(+) 0.32[a]	(+) 0.35	(−) 0.18	(−) 0.20	0.15
$\langle\langle R\rangle\rangle$	0.14 ± 0.39	0.23 ± 0.35	-0.13 ± 0.18	-0.16 ± 0.15	0.00 ± 0.18
scale factor[b]	1.38	1.70	0.75	0.69	1

[a] The values indicate 1 standard deviation. [b] "Scale Factor" is $10^{\langle\langle R\rangle\rangle}$, which indicates the average factor by which the single-wavelength times differ from the spectral-reconstruction times.

Table 3. These final results provide an indication of the accuracy to be expected when using the single-wavelength method in the manner recommended here. From the rows labeled no. $\langle|R|\rangle$, one finds that for 67% (16/24) of the solvents examined, the times derived from $S_{LW}^{560}(1.35 \cdot t)$ lie within a factor of 1.5 of the spectral-reconstruction times (i.e., the predicted times are either too small or too large by this factor). The standard deviation of ± 0.18 in $\langle\langle R\rangle\rangle$ also indicates this same level of scatter (a factor of 1.5) about the spectral-reconstruction results. It should be noted that the uncertainties in the spectral-reconstruction measurements are not negligible compared to these values. Uncertainties in spectral-reconstruction times were estimated to be at least $\pm 15-25\%$ for the $1/e$ times and larger than 25% for other times characterizing the short- and long-time behavior of $S_\nu(t)$.[21] Taking these uncertainties into account, a reasonable estimate of the accuracy with which the single-wavelength method can be expected to reproduce exact spectral reconstruction results is $\pm 30-40\%$ (1 standard deviation).

VII. Summary and Conclusions

Extensive steady-state and time-resolved data have been used to evaluate the accuracy of the single-wavelength method for reproducing the spectral response functions, $S_\nu(t)$, of the solvation probe coumarin 153. The essential findings from this study may be summarized as follows. No observation wavelength was found for which the spectral-density function is linear over the entire wavelength range important in dynamical measurements. Approximately linear behavior was found for two observation wavelengths, 476 nm ("blue") and 556 nm ("red"), and these two wavelengths were used to estimate $S_\nu(t)$. As expected from the better linearity of the 556-nm spectral densities, response functions estimated using the linear version of the single-wavelength approximation and the 560-nm "linear" wavelength reproduce the spectral-reconstruction results much more accurately than those measured at 470 nm. This finding is noteworthy in light of the fact that 480 nm was originally recommended as the optimum choice for C153[23] and it has been used in subsequent work.[38] The present results indicate that the solvation times obtained in this manner could be in substantial error. Fortunately, most prior work involved moderately polar solvents, whose emission frequencies fall within a region where the errors are not as severe as those for less polar or the most strongly polar solvents. (In the latter cases, errors larger than a factor of 2 are common.) Errors made using the 470-nm and to a lesser extent the 560-nm observation wavelength are correlated to the frequencies over which the spectral dynamics occur. These correlations can be rationalized in terms of the degree of curvature (i.e., nonlinearity) present in the respective spectral-density functions over the frequency range of the dynamical

shift. However, application of the more general, nonlinear version of the single-wavelength method does not significantly improve agreement between the single-wavelength predictions and the spectral-reconstruction results. Therefore the final recommendation made in this work is to use the linear version of the single-wavelength method at an observation wavelength of 555−560 nm. To account for a systematic underestimation of the times made using this approach, it is further recommended that $S_\nu(t)$ be approximated by the relation: $S_\nu(t) \cong S_{LW}(1.35 \cdot t)$. The comparisons made here suggest that spectral-response times determined in this manner can be expected to be accurate to the level of roughly ±30−40%, where this value represents one standard deviation (i.e., a 68% confidence limit) in a typical measurement.

Several further observations can be made on the basis of the data presented here. First, while the single-wavelength method is perhaps not as accurate as might be hoped, the fact that the method works as well as it does provides strong support for the fundamental assumptions on which it is based. In the case of C153, the smooth appearance of the spectral-density plots (Figure 4) is consistent with the idea that a single variable ("polarity") is sufficient to characterize all of the attributes of the steady-state emission spectra in quite a wide range of solvents. The notion that the dynamic evolution of the emission spectrum during solvation in a single solvent is comparable to the evolution of suitably normalized steady-state spectra as a function of increasing solvent polarity is also a good first approximation (Figure 3). However, time-evolving spectra are predicted and observed to undergo changes in shape, most notably width changes, that make the agreement between the steady-state and time-evolving spectra imperfect, especially at early times. It is reasonable to attribute the lack of improved agreement with spectral-reconstruction results using the nonlinear version of the single-wavelength method to these inherent differences in dynamic and equilibrium spectra.

The single-wavelength method is perhaps best viewed as complementary to the spectral-reconstruction method for measuring solvation times. Complete spectral reconstruction provides a true record of how the spectrum evolves in time, and the average frequency of this spectrum is the most direct measure of the solvation energy relaxation. Thus, spectral reconstruction is certainly the method of choice when accurate results are required or when unusual conditions prevail. Spectral-reconstruction results can also be compared with independent estimates of the position of the time-zero spectrum,[21] enabling a determination of how much, if any, of the solvation response has been missed due to limited experimental time resolution. No similar check upon the results obtained using the (linear) single-wavelength method is possible, and therefore solvation components faster than the instrumental resolution are necessarily omitted from single-wavelength estimates of $S_\nu(t)$. However, spectral reconstruction is not without drawbacks. Besides the much greater effort entailed in collecting the requisite number of decays for spectral reconstruction, independent fitting of emission transients at different wavelengths can sometimes lead to subtle artifacts in $S_\nu(t)$. Possible examples of such artifacts can be found in ref 21, where small-amplitude (<10%) long-time tails in some $S_\nu(t)$ functions of uncertain origin were reported. Although these tails do not appreciably distort $S_\nu(t)$ at most times, they do have a large impact on the integral solvation times important in some applications.[39] The absence of such tails in the single-wavelength estimates bolsters the suspicion that these tails do not represent true solvation components. Thus, as this example shows, examining single-wavelength predictions when carrying out complete spectral-reconstruction analysis can provide a useful check on the reconstruction procedure. A more obvious use for the single-wavelength method is in situations where solvation dynamics in a series of related solvent conditions must be measured. For example, one might be interested in binary solvent systems as a function of composition,[23,40] isotope substitution[41,42] or at a series of different pressures or temperatures.[43] In such cases, better precision is expected from the single-wavelength estimates of $S_\nu(t)$ compared to those of spectral reconstruction, since the data required in the former case can be recorded in a short period of time with fixed instrumental parameters. Even if the ultimate accuracy is less than that obtained from spectral reconstruction, the relative changes observed using the single-wavelength method should be reliable as long as the frequency range which spans the spectral dynamics does not vary greatly across the series.

Acknowledgment. This work was supported by funds from the Division of Basic Energy Sciences of the U.S. Department of Energy. We thank Dr. Miin-Liang Horng for his help in acquiring the data on which the present work is based and Paul Barbara for suggesting that we undertake these comparisons.

References and Notes

(1) Maroncelli, M. *J. Mol. Liq.* **1993**, *57*, 1.
(2) Barbara, P. F.; Jarzeba, W. *Adv. Photochem.* **1990**, *15*, 1.
(3) Bagchi, B.; Biswas, R. *Acc. Chem. Res.* **1998**, *31*, 181.
(4) Horng, M.-L.; Gardecki, J. A.; Maroncelli, M. *J. Phys. Chem. A* **1997**, *101*, 1030.
(5) Hartman, R. S.; Konitsky, W. M.; Waldeck, D. H.; Chang, Y. J.; Castner, E. W. *J. Chem. Phys.* **1997**, *106*, 7920.
(6) Rey, R.; Hynes, J. T. *J. Chem. Phys.* **1998**, *108*, 142.
(7) Hamm, P.; Lim, M.; Hochstrasser, R. M. *J. Chem. Phys.* **1997**, *107*, 10523.
(8) Hynes, J. T. In *Ultrafast Dynamics of Chemical Systems*; Simon, J. D., Ed.; Klewer: Dordrecht, 1994; p 345.
(9) Heitele, H. *Angew. Chem., Int. Ed. Engl.* **1993**, *32*, 359.
(10) Nishiyama, K.; Okada, T. *J. Phys. Chem. A* **1997**, *101*, 5729.
(11) Ma, J.; Van Bout, D.; Berg, M. *J. Chem. Phys.* **1995**, *103*, 9146.
(12) Kovalenko, S. A.; Ruthmann, J.; Ernsting, N. P. *Chem. Phys. Lett.* **1997**, *266*, 40. Kovalenko, S. A.; Ruthman, J.; Ernsting, N. P. *J. Chem. Phys.* **1998**, *109*, 1894.
(13) Passino, S. A.; Nagasawa, Y.; Joo, T.; Fleming, G. R. *J. Phys. Chem. A* **1997**, *101*, 725.
(14) d. Boeij, W. P.; Pschenichnikov, M. S.; Wiersma, D. A. *J. Phys. Chem.* **1996**, *100*, 11806.
(15) Yang, T.-S.; Vohringer, P.; Arnett, D. C.; Scherer, N. F. *J. Chem. Phys.* **1995**, *103*, 8346.
(16) Joo, T.; Jia, Y.; Yu, J.-Y.; Lang, M. J.; Fleming, G. R. *J. Chem. Phys.* **1996**, *104*, 6089.
(17) Fainberg, B. D.; Huppert, D. *J. Mol. Liq.* **1995**, *64*, 123.
(18) Castner, E. W.; Maroncelli, M. *J. Mol. Liq.* **1998**, *77*, 1.
(19) Maroncelli, M.; Fleming, G. R. *J. Chem. Phys.* **1987**, *86*, 6221.
(20) Gardecki, J.; Horng, M.-L.; Papazyan, A.; Maroncelli, M. *J. Mol. Liq.* **1995**, *65/66*, 49.
(21) Horng, M. L.; Gardecki, J. A.; Papazyan, A.; Maroncelli, M. *J. Phys. Chem.* **1995**, *99*, 17311.
(22) Kahlow, M. A.; Jarzeba, W.; Kang, T. J.; Barbara, P. F. *J. Chem. Phys.* **1989**, *90*, 151.
(23) Jarzeba, W.; Walker, G. C.; Johnson, A. E.; Barbara, P. F. *Chem. Phys.* **1991**, *152*, 57.
(24) Reynolds, L.; Gardecki, J. A.; Frankland, S. J. V.; Horng, M. L.; Maroncelli, M. *J. Phys. Chem.* **1996**, *100*, 10337.
(25) Maroncelli, M. *J. Chem. Phys.* **1997**, *106*, 1545.
(26) It must be admitted that not everyone believes C153 to be an ideal solvation probe. Some researchers have considered the possibility of multiple excited electronic states playing a role in the dynamics. See the discussion in ref 34 for details.
(27) Nagarajan, V.; Brearley, A. M.; Kang, T. J.; Barbara, P. F. *J. Chem. Phys.* **1987**, *86*, 3183.
(28) Kahlow, M. A.; Kang, T. J.; Barbara, P. F. *J. Chem. Phys.* **1988**, *88*, 2372.
(29) van der Zwan, G.; Hynes, J. T. *J. Phys. Chem.* **1985**, *89*, 4181.
(30) Fee, R. S.; Maroncelli, M. *Chem. Phys.* **1994**, *183*, 235.
(31) Maroncelli, M. *J. Chem. Phys.* **1991**, *94*, 2084.

(32) Carter, A. E.; Hynes, J. T. *J. Chem. Phys*. **1991**, *94*, 5961.
(33) Ando, K. *J. Chem. Phys*. **1991**, *94*, 2084.
(34) Lewis, J. E.; Maroncelli, M. *Chem. Phys. Lett*. **1998**, *282*, 197.
(35) In ref 34, the solvent dependence of the radiative rate was actually found to be proportional to the product $n^3\tilde{\nu}^3$ where n is the refractive index of the solvent and $\tilde{\nu}^3$ is the inverse of the average of ν^{-3}. However, use of the simple-average frequency and neglect of the refractive-index factor still provides results in accord with eq 13 to ±10%.
(36) It should be noted that in addition to performing detailed analysis of these two wavelengths, we also surveyed all wavelengths available to ensure that the ones chosen were indeed the most appropriate for representing $S_\nu(t)$.
(37) The uncertainty in the 1/e times from spectral reconstruction was estimated to be ±(15−25)%. See ref 21 for more details.
(38) Actually, Huppert and co-workers adopted a wavelength of 460 nm for C153 in their studies of solvation in ionic solutions: Ittah, V.; Huppert, D. *Chem. Phys. Lett*. **1990**, *173*, 496. Bart, E.; Meltsin, A.; Huppert, D. *Chem. Phys. Lett*. **1992**, *200*, 592.
(39) For example, in considering dielectric-friction effects, one needs the integral solvation time. The most recent dielectric continuum comparisons made to the spectral reconstruction results in ref 25 indicate that the small-amplitude long-time tails reported for the *N*-methyl amides may not be real solvation components.
(40) Gardecki, J. A.; Maroncelli, M. Solvation and Rotational Dynamics in Acetonitrile/Propylene Carbonate Mixtures: A Binary System for Use in Dynamical Solvent-Effect Studies. *Chem. Phys. Lett*., in press.
(41) Shirota, H.; Pal, H.; Tominaga, K.; Yoshihara, K. *J. Phys. Chem*. **1996**, *100*, 1475.
(42) Pal, H.; Nagasawa, Y.; Tominaga, K.; Kumazaki, S.; Yoshihara, K. *J. Chem. Phys*. **1995**, *102*, 7758.
(43) Nagasawa, Y.; Yartsev, A. P.; Tominaga, K.; Johnson, A. E.; Yoshihara, K. *J. Chem. Phys*. **1994**, *101*, 5717.